

Hybrid Poly(β -amino ester) Triblock Copolymers Utilizing a RAFT Polymerization Grafting-From Methodology

Karolina Kasza, Amr Elsherbeny, Cara Moloney, Kim R. Hardie, Miguel Cámara, Cameron Alexander, and Pratik Gurnani*

The biocompatibility, biodegradability, and responsiveness of poly(β -amino esters) (PBAEs) has led to their widespread use as biomaterials for drug and gene delivery. Nonetheless, the step-growth polymerization mechanism that yields PBAEs limits the scope for their structural optimization toward specific applications because of limited monomer choice and end-group modifications. Moreover, to date the post-synthetic functionalization of PBAEs has relied on grafting-to approaches, challenged by the need for efficient polymer–polymer coupling and potentially difficult post-conjugation purification. Here a novel grafting-from approach to grow reversible addition–fragmentation chain transfer (RAFT) polymers from a PBAE scaffold is described. This is achieved through PBAE conversion into a macromolecular chain transfer agent through a multistep capping procedure, followed by RAFT polymerization with a range of monomers to produce PBAE–RAFT hybrid triblock copolymers. Following successful synthesis, the potential biological applications of these ABA triblock copolymers are illustrated through assembly into polymeric micelles and encapsulation of a model hydrophobic drug, followed by successful nanoparticle (NP) uptake in breast cancer cells. The findings demonstrate this novel synthetic methodology can expand the scope of PBAEs as biomaterials.

1. Introduction

Poly(β -amino esters) (PBAEs) have recently attracted considerable attention due to their inherent biocompatibility, biodegradability, responsiveness, and structural versatility.^[1] Synthesized through a one-pot aza-Michael addition of primary or secondary amines with diacrylates, PBAEs are equipped with hydrolytically degradable ester bonds supporting their use as biomaterials. Furthermore, the inherent tertiary amine groups permit their use for carrying negatively charged cargo or as pH responsive materials.^[2] Accordingly, these advantages mean PBAEs have been widely explored in areas such as drug, gene, and vaccine delivery, particularly when assembled into micelles or polyelectrolyte complexes.^[1,3–8]

However, the step-growth polymerization mechanism that yields PBAEs means that structure optimization toward specific applications must either come from the limited amine and diacrylate monomer choice or via end-group modification. Meanwhile other polymerization techniques, such as controlled radical polymerizations or ring opening polymerizations, can easily control block length and sequence for nanoparticle formulation. This is particularly significant for tuning the surface chemistries of


K. Kasza, A. Elsherbeny, C. Alexander
Division of Molecular Therapeutics and Formulation
School of Pharmacy
University of Nottingham
Nottingham NG7 2RD, UK

K. Kasza, K. R. Hardie, M. Cámara
National Biofilms Innovation Centre
School of Life Sciences, Biodiscovery Institute
University Park, University of Nottingham
Nottingham NG7 2RD, UK

A. Elsherbeny
Ex Vivo Cancer Pharmacology Centre of Excellence
School of Medicine
University of Nottingham
Nottingham NG7 2RD, UK

A. Elsherbeny, C. Moloney
School of Medicine
Biodiscovery Institute
University Park, University of Nottingham
Nottingham NG7 2RD, UK

P. Gurnani
UCL School of Pharmacy
University College London
29–39 Brunswick Square, London WC1N 1AX, UK
E-mail: p.gurnani@ucl.ac.uk

 The ORCID identification number(s) for the author(s) of this article can be found under <https://doi.org/10.1002/macp.202300262>

© 2023 The Authors. Macromolecular Chemistry and Physics published by Wiley-VCH GmbH. This is an open access article under the terms of the Creative Commons Attribution License, which permits use, distribution and reproduction in any medium, provided the original work is properly cited.

DOI: 10.1002/macp.202300262

nanomaterials in applications where stabilization in physiological fluids or targeting to specific cell types is required.^[8,9] Surprisingly, no simple strategy to tune the surface chemistries for PBAE nanoparticles has yet been reported, despite their widespread use as a biomaterial. The current state of the art relies on post-polymerization grafting of pre-synthesized polymers such as poly(ethylene glycol) (PEG)^[10,11] onto reactive handles at the chain end of prepared PBAEs, with copolymerization shown to enhance stability and promote efficacy in both the context of gene and drug delivery. Kim et al.^[10] reported the synthesis of PEG–PBAE–PEG triblock copolymers, for gene delivery, with a prolonged particle stability and improved efficacy observed in vivo. Thambi et al.^[12] demonstrated a methodology to obtain PBAEs with hyaluronic acid attached, with an improvement in doxorubicin efficacy and a decrease in toxicity reported. Moreover, Cordeiro et al.^[13] reported high-buffering capacities and efficient pDNA delivery for (2-(dimethylamino)ethyl methacrylate)-PBAE-(2-(dimethylamino)ethyl methacrylate) triblock copolymers. In each case, polymer attachment was undertaken through a grafting-to approach, relying on efficient polymer–polymer coupling and potentially challenging post-conjugation purification. We postulated that a grafting-from approach to grow polymers from a PBAE scaffold would enable access to a new class of PBAE, expanding their scope in biomedical applications.

Grafting-from strategies have previously been explored with compounds such as cyclic peptides,^[14] cellulose,^[15] and proteins^[16] primarily utilizing reversible deactivation radical polymerization techniques. Of these, reversible addition–fragmentation chain transfer (RAFT) polymerization has been especially popular for grafting-from methodologies due to its molar mass control, ambient polymerization conditions, monomer versatility, orthogonality with common functional moieties, and importantly, ability to create macroinitiators to extend.^[17]

Therefore, in this study we propose a new class of block copolymer produced via a grafting-from methodology utilizing RAFT polymerization to functionalize PBAEs. Hence, we enable synthesis of PBAE triblock copolymers, utilising a PBAE core with a versatile range of graft polymers both ends of the PBAE chain, therefore expanding the scope of PBAEs as biomaterials. Initially, we describe the development of PBAE macromolecular chain transfer agents through a multi-step capping procedure, followed by RAFT polymerization with a range of monomers to produce PBAE–RAFT hybrid triblock copolymers. Following successful synthesis, we then illustrate their potential biological applications through assembly into polymeric micelles, encapsulation of a model hydrophobic drug and demonstration of successful nanoparticle (NP) uptake in breast cancer cells.

2. Experimental Section

2.1. Materials

Butanediol diacrylate (BDD), hexanediol diacrylate (HDD), 3-aminopropanol (3AP), piperazine (PIP), triethylamine (TEA), 2-acrylamido-2-methylpropane sulfonic acid (AMPS), dimethyl

sulfoxide (DMSO)-d₆ (99.5% D atom), chloroform-d (99.8% D atom), 4,4'-azobis(4-cyanovaleric acid) (ACVA, >98%), docetaxel (DTX) (99.8% pure), Roswell Park Memorial Institute media (RPMI), trypsin-EDTA solution, fetal bovine serum (FBS), L-glutamine were obtained from Sigma-Aldrich without further purification. N-Acryloyl morpholine (NAM), N,N-dimethylacrylamide (DMA), acrylic acid (AA), and 2-(N,N-dimethyl amino) ethyl acrylate (DMAEA) were all purchased from Sigma-Aldrich and the inhibitor removed by passing the monomers through a column of basic aluminum oxide. Formvar carbon 200 mesh and graphene oxide grids were purchased from Agar Scientific. PrestoBlue Cell Viability Reagent was purchased from ThermoFischer Scientific. LumiTracker Lyso Green fluorescent dye was purchased from Lumiprobe. Acryloxyethyl thiocarbonyl Rhodamine B was purchased from Polysciences, Inc. Solvents and other reagents were acquired from commercial sources and used as received unless stated otherwise.

2-(((Butylthio)carbonothioyl)thio)propanoic acid (PABTC) and N-hydroxysuccinamide-(propanoic acid)yl butyl trithiocarbonate (NHS-PABTC) were synthesized by methods previously reported in literature.^[14,18]

2.2. Methods

2.2.1. Instrumentation and Analysis

NMR Spectroscopy: ¹H NMR spectra were recorded on a Bruker DPX-400 spectrometer using deuterated solvent (materials section).

Size Exclusion Chromatography (SEC): A Polymer Laboratories PL-50 instrument equipped with differential refractive index (DRI) was used for SEC analysis. The system was fitted with 2× PLgel Mixed D columns (300 × 7.5 mm) and a PLgel 5 μm guard column. The eluent used was DMF with 0.1% LiBr. Samples were run at 1 mL min⁻¹ at 50 °C. Poly(methyl methacrylate) standards (Agilent EasyVials) were used for calibration between 955,500 and 550 g mol⁻¹. Analyte samples were filtered through a membrane with 0.22 μm pore size before injection. Experimental molar mass (M_n,SEC) and dispersity (Đ) values of synthesized polymers were determined by conventional calibration using Cirrus GPC software.

Dynamic Light Scattering: Dynamic light scattering (DLS) measurements were measured using a Malvern Zetasizer Nano ZS apparatus equipped with a He–Ne laser operated at λ = 633 nm and at a scattering angle of 173°. Particle size was measured at concentrations of 1 mg mL⁻¹ in water at 25 °C, with three scans taken per measurement.

Transmission Electron Microscopy (TEM) Characterization: An aliquot (13 μL) of nanoparticles in water (1 mg mL⁻¹) was deposited onto a Formvar carbon 200 mesh grid for DMA₁₅₀–(HDD-PIP)–DMA₁₅₀ particles or a graphene oxide grid for NAM₁₅₀–(HDD-PIP)–NAM₁₅₀ particles for 1 min and then the grid was blotted with filter paper (Fisherbrand, Grade 12). The sample was negatively stained with a 2% uranyl acetate solution in water (13 μL) for 1 min, and then the grid was again blotted with filter paper (Fisherbrand, Grade 12) and dried in air. Transmission electron microscopy analyses were carried out using a FEI Tecnai microscope using an accelerating voltage of 100 kV.

Theoretical Molar Mass Calculation:

$$M_{n,th} = M_0 \frac{1+r}{(1+r-2rp)} \quad (1)$$

Equation 1: Calculation of theoretical number average molar mass ($M_{n,th}$) according to Carothers equation, where M_0 is the molar mass of the repeating polymer unit, r the stoichiometric ratio of diacrylate to amine and p the degree of polymerization which is assumed as 1. It is used to calculate the theoretical molar mass of PBAEs.

$$M_{n,th} = \frac{[M]_0 p M_M}{[CTA]_0} + M_{CTA} \quad (2)$$

Equation 2: Calculation of theoretical number average molar mass ($M_{n,th}$) where $[M]_0$ and $[CTA]_0$ are the initial concentrations (in mol dm⁻³) of monomer and chain transfer agent respectively. p is the monomer conversion as determined by ¹H NMR spectroscopy. M_M and M_{CTA} are the molar masses (g mol⁻¹) of the monomer and chain transfer agent respectively. It is used to calculate the theoretical molar mass of the PBAE-RAFT ABA tri-block copolymers.

2.2.2. PBAE Synthesis

PBAEs were synthesized as previously reported.^[19] Butanediol diacrylate (5 g, 25.2 mmol) or hexanediol diacrylate (10 g, 44.2 mmol) was mixed with amine at a 1.1:1 molar ratio of monomer to amine in either DMSO (BDD-3AP polymer) or dioxane (HDD-PIP polymer) at 500 mg mL⁻¹ and the reaction stirred in the dark at 90 °C for 24 h. Following reaction completion, the mixture was diluted (167 mg mL⁻¹) and end-capped using 2,2-(ethylenedioxy)diethylamine (0.5 M) at 25 °C for 24 h. The resulting polymer was purified in tetrahydrofuran (THF), and diethyl ether (1:9) and the solvent removed under reduced pressure to yield a yellow, viscous liquid. Amine capping efficacy was assessed using ¹H NMR with no acrylate peaks present following the capping steps. The final polymers were characterized by SEC and ¹H NMR.

PBAE Functionalization with NHS-PABTC: The selected PBAE (1 g, 1 eq.) and NHS-PABTC (6 eq.) were solubilized in DMF (1 mg mL⁻¹ final PBAE concentration) following which TEA (3 eq.) was added. The reaction was left to stir (450 rpm, 25 mm stirrer bar) in the dark at 25 °C for 48 h. Following reaction completion, the resulting PBAE-mCTAs were purified in THF and diethyl ether (1:9), and the solvent was removed under reduced pressure yielding the PBAE-mCTAs as yellow, viscous liquids. The final polymers were analyzed by SEC and ¹H NMR.

2.2.3. Grafting-From RAFT Polymerization

RAFT polymer chain extension was conducted in dioxane under nitrogen with the selected monomers (1.5 M), selecting degrees of polymerization (DP) of 100, 200, and 300; using ACVA (10 mg mL⁻¹ stock in dioxane) as the initiator and keeping the CTA to initiator ratio as 2. The reaction was left to stir under

nitrogen at 70 °C for 24 h. The resulting polymers were analyzed using ¹H NMR and SEC. Conversion was assessed using ¹H NMR by comparing the integration of the acrylate/acrylamide peaks before and after reaction completion, using the PBAE polyester protons a 4.01 ppm as a reference. Rhodamine-tagged polymers were synthesized by adding an acryloxyethyl thiocarbonyl rhodamine B stock solution in DMF (10 µg mL⁻¹) to the reaction mixture, targeting a 0.1% molar dye content in total number of monomer moles used.

2.2.4. PBAE-RAFT Particle Formulation

Micelle Formulation by Solvent Precipitation: Micelles were formulated by adding the polymer solution (100 µL, 10 mg mL⁻¹) in acetone or THF to Mili-Q grade water (1 mL) in a scintillation vial (20 mL) at a rate of 0.1 mL min⁻¹ under constant stirring (960 rpm, 25 mm stirrer bar) to yield a final polymer concentration of 1 mg mL⁻¹. The suspension was left to stir for 1 h following which the organic solvent was removed under reduced pressure.

Micelle Formulation by Direct Water Solubilization: Micelles were formulated by adding Mili-Q grade water (5 mL) to dry polymer (5 mg) in a scintillation vial (20 mL), under constant stirring (960 rpm, 25 mm stirrer bar) and suspension being left to stir for 1 h, to yield a final polymer concentration of 1 mg mL⁻¹.

2.2.5. Drug Encapsulation

Mili-Q grade water (5 mL) and a docetaxel (DTX) solution in dimethyl sulfoxide (DMSO) (0.5 mL, 5 mg mL⁻¹) were simultaneously added to weighed out polymer (5 mg) and left to stir (960 rpm, 25 mm stirrer bar) for 2 h to yield a final polymer concentration of 1 mg mL⁻¹. Centrifugal filtration (3500 Dalton molecular weight cutoff, Amicon) was applied to purify the unencapsulated drug. The experiments were repeated three times, each time using three technical replicates.

Quantification of Drug Load by HPLC: Drug-loaded particles (5 mL) were freeze-dried for 24 h (0.98 mbar), dissolved in a 50:50 mixture of DMSO and trifluoroacetic acid (TFA), and left to stir for 3 h. The solution was then diluted 1:10 in DMSO and encapsulation levels were assessed by high performance liquid chromatography (HPLC) (Agilent Technologies 1200 series, USA). The experiment was repeated three times, each time using three technical replicates.

Drug loading of DTX was assessed using a C18 (4.6 × 250 mm; 5 µm) analytical column (ZORBAX Eclipse Plus). The UV detector was operated at 239 nm. The mobile phase consisted of a mixture of 0.1% orthophosphoric acid aqueous solution and ACN (40:60, v/v). The flow rate was set at 1.0 mL min⁻¹ and injection volume at 25 µL.^[20]

Drug loading and encapsulation efficiency were calculated using the following equations:

$$\text{Drug loading (\%)} = \frac{\text{Weight of loaded drug}}{\text{Total weight of polymer}} \times 100 \quad (3)$$

Equation 3: Calculation of percentage drug load.

$$\text{Drug encapsulation \%} \left(\frac{w}{w} \right) = \frac{\text{Total amount of drug} - \text{unloaded drug}}{\text{Total amount of drug}} \times 100 \quad (4)$$

Equation 4: Calculation of percentage drug encapsulation.

2.2.6. Docetaxel Release Study

DTX release from polymer carrier was assessed in phosphate buffer at pH = 7.4, containing 0.25% Tween 20. A sample (2.5 mL, 2 mg mL⁻¹) of DTX-loaded nanoparticles was placed in a dialysis membrane (3500 Dalton molecular weight cutoff, Spectrum Labs) The micellar solution was dialyzed against 30 mL of release media at 37 °C, over 72 h, and samples (1 mL) were collected at appropriate timepoints and replaced with the same amount of fresh medium to maintain sink conditions. DTX quantification from the release samples was conducted by HPLC as described above.

2.2.7. Cell Culture of MDA-MB-231 Cells

The MDA-MB-231 triple-negative breast cancer cell lines were obtained from the American Type Culture Collection (Manassas, VA). These cell lines were cultured in Roswell Park Memorial Institute (RPMI) medium supplemented with 10% (v/v) fetal bovine serum (FBS) and 2 mM L-glutamine. The cultures were incubated at 37 °C in a 5% CO₂ environment. When the cell monolayers reached 80% confluency, the cancer cells were detached using 1× Trypsin-EDTA solution (Sigma-Aldrich Co., St. Louis, MI, USA). To determine the live cell number, an aliquot from the cell suspension was stained with Trypan blue (Sigma-Aldrich Co., St. Louis, MI, USA) under an optical microscope. This staining allowed for the identification of dead cells, while the remaining unstained cells were counted using a hemocytometer.

2.2.8. Uptake in 2D Monolayers of MDA-MB-231 Cells

MDA-MB-231 cells were seeded in CellView 35 mm diameter glass bottom cell culture dishes at a density of 2.5 × 10⁵ cells per dish and cultured for 24 h in RPMI. Then, the media was removed, and 50 µg mL⁻¹ rhodamine-labeled nanoparticles were added and incubated with cells for 4 h at 37 °C with 5% CO₂. Following exposure, nanoparticle solutions were removed, and cells were washed three times with ice-cold phosphate-buffered saline (PBS). Cells were then stained with 10 µg mL⁻¹ Hoechst 33342 (Thermo-Fisher) for 15 min and washed three times with ice-cold PBS. Afterwards, 75 nm LumiTracker Lyso Green (Lumiprobe) was applied in PBS for 30 min before the staining solution was finally removed and the cells washed twice with PBS. Subsequently, the cells were imaged using Leica TCS SPE laser scanning confocal microscope. The images were processed using ImageJ software and the JACoP (Just Another Colocalisation Plugin) in ImageJ was used for the calculation of Pearson's correlation coefficient for co-localization studies.^[21]

Table 1. Molar mass characterization of PBAE and PBAE-mCTAs. Polymer ¹H NMR and SEC characterization is available in Figures S2 and S3 (Supporting Information).

Polymer	$M_{n,th}$ [g mol ⁻¹] ^{a)}	$M_{n,SEC}$ [g mol ⁻¹] ^{b)}	\bar{D}
BDD-3AP	5800	6000	1.40
BDD-3AP-mCTA	6302	9200	1.72
HDD-PIP	6700	14000	1.43
HDD-PIP-mCTA	7200	18000	1.37

^{a)} Calculated using Equation 1; ^{b)} Determined using DMF-SEC.

2.2.9. Cytotoxic Activity in 2D Monolayers of MDA-MB-231 Cells

MDA-MB-231 cells were seeded in tissue culture treated Thermo Scientific Nunc MicroWell 96-Well Optical-Bottom black plates at a density of 1 × 10⁴ cells per well and cultured for 24 h in RPMI. The media was then removed, and the cells treated with different concentrations of blank NAM₁₅₀-(HDD-PIP)-NAM₁₅₀ and DMA₁₅₀-(HDD-PIP)-DMA₁₅₀ nanoparticles for 72 h. Subsequently, the treatments were replaced with 100 µL of 10% PrestoBlue HS Cell Viability Reagent in RPMI and incubated for 20 min. The fluorescence intensity was measured using an excitation/emission wavelength of 544/590 nm on a FLUOstar Omega plate reader (BMG LABTECH, UK).

3. Results and Discussion

3.1. Development of Synthetic Methodology

To develop our grafting-from methodology we first synthesized two PBAE models via traditional one-pot aza-Michael addition chemistry. A hydrophilic butanediol diacrylate (BDD)- 3-amino propan-1-ol (3AP) copolymer, and a hydrophobic hexanediol diacrylate (HDD)- piperazine (PIP) copolymer utilizing 1.1:1 diacrylate:amine ratio, using previously reported conditions.^[19] Both polymers displayed molar masses close to the theoretical value calculated via Carothers equation and exhibited residual acrylate signals in the ¹H NMR spectra (Table 1). The terminal acrylates were then end-capped with an excess of (2,2-(ethylenedioxy)diethylamine) to avoid any PBAE coupling. The final amino functional PBAEs displayed similar molar masses to their acrylate terminated analogs while full amine functionalization was confirmed by the complete disappearance of the acrylate signals in the ¹H NMR spectra. For the HDD-PIP polymer, we observed an increase in molar mass following polymer purification in a mixture of THF and cold ether (1:9), hypothesized to be caused by the solubility of lower molar mass chains in the purification solvent leading to their removal during this step. The amino terminated hydrophobic and hydrophilic PBAEs were then further functionalized at the α and ω end groups with an N-hydroxysuccinimide functional RAFT agent, NHS-PABTC, to form PBAE macromolecular chain transfer agents (PBAE-mCTA) (Figure 1; Figure S1, Supporting Information). Following CTA functionalization, we observed a further increase in $M_{n,SEC}$, particularly for the HDD-PIP polymer, hypothesized to originate from the solubilization of lower molar mass chains in the purification solvent.

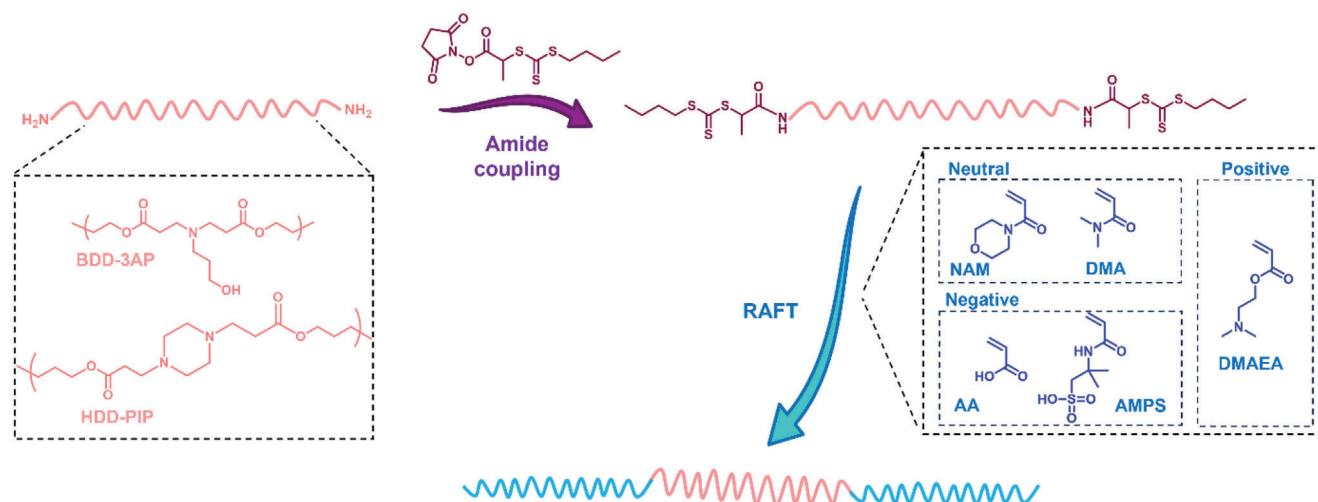


Figure 1. Outline of the synthetic methodology developed to make PBAE-RAFT triblock copolymers, including the structural details of the core PBAE scaffolds used and RAFT comonomers tested.

In order to produce triblock copolymers efficiently via our grafting-to methodology, it was imperative to ensure the PBAE-mCTAs expressed RAFT agents at both ends on all PBAE molecules, as any proportion of monofunctionalized PBAE-mCTA would result in bimodal molar mass distribution for the resultant triblock copolymers (Figure 2a). To optimize this

process, we tested different PBAE:NHS-PABTC equivalents (2–6 eq.) and PBAE:triethylamine equivalents (0–3 eq.) for this reaction. Unfortunately, NHS-PABTC attachment was not easily detectable via ^1H NMR spectroscopy, hence to assess functionalization efficiency we postulated that the shape of the molar mass distribution following RAFT polymerization would illustrate the

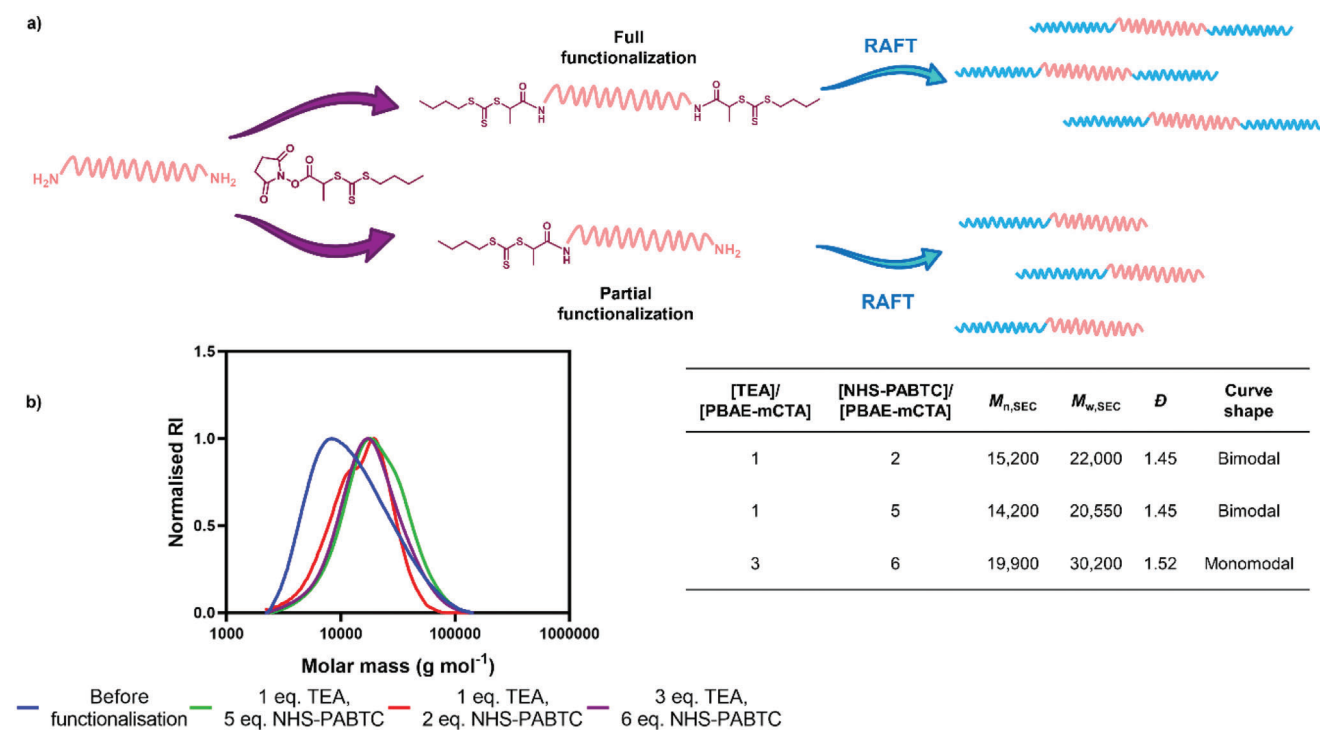


Figure 2. Optimization of synthetic methodology used to synthesize the PBAE-mCTA, based on NAM_{50} -(BDD-3AP)- NAM_{50} molar mass distributions (g mol^{-1}), where a) outline of full and partial PBAE functionalization with NHS-PABTC and the resulting copolymer structures; b) molar mass distributions of NAM_{50} -(BDD-3AP)- NAM_{50} defined by $M_{n,SEC}$ where final polymer was synthesized using 1 eq. of TEA and 2 eq. of NHS-PABTC (red); 1 eq. of TEA and 5 eq. of NHS-PABTC (green); and 3 eq. of TEA and 6 eq. of NHS-PABTC (purple); Inset table contains the comparison of final NAM_{50} -(BDD-3AP)- NAM_{50} polymer number average molar mass (M_n), weight average molar mass (M_w), polydispersity (\mathcal{D}), and curve shape depending on TEA and NHS-PABTC equivalents used to synthesize the starting PBAE-mCTA.

Table 2. Characterization of PBAE–RAFT ABA-triblock copolymers. Polymer ¹H NMR and SEC characterization is available in Figures S3 and S4 (Supporting Information).

Polymer	DP _{target}	Conversion %	M _{n, th} [g mol ⁻¹] ^{a)}	M _{n, SEC} [g mol ⁻¹] ^{b)}	Đ
NAM ₅₀ -(BDD-3AP)-NAM ₅₀	100	100%	23 600	20 000	1.52
DMA ₅₀ -(BDD-3AP)-DMA ₅₀	100	98%	19 200	18 000	1.25
AA ₅₀ -(BDD-3AP)-AA ₅₀	100	78%	N/A	N/A	N/A
AMPS ₅₀ -(BDD-3AP)-AMPS ₅₀	100	PBAE degradation	N/A	N/A	N/A
DMAEA ₅₀ -(BDD-3AP)-DMAEA ₅₀	100	14%	N/A	N/A	N/A
NAM ₅₀ -(HDD-PIP)-NAM ₅₀	100	91%	30 800	28 000	1.74
DMA ₅₀ -(HDD-PIP)-DMA ₅₀	100	97%	27 600	27 000	1.64
AA ₅₀ -(HDD-PIP)-AA ₅₀	100	PBAE degradation	N/A	N/A	N/A
AMPS ₅₀ -(HDD-PIP)-AMPS ₅₀	100	23%	N/A	N/A	N/A
DMAEA ₅₀ -(HDD-PIP)-DMAEA ₅₀	100	41%	N/A	N/A	N/A
NAM ₁₀₀ -(HDD-PIP)-NAM ₁₀₀	200	99%	45 900	33 000	1.84
DMA ₁₀₀ -(HDD-PIP)-DMA ₁₀₀	200	98%	37 400	33 000	1.94
NAM ₁₅₀ -(HDD-PIP)-NAM ₁₅₀	300	99%	59 900	39 000	1.94
DMA ₁₅₀ -(HDD-PIP)-DMA ₁₅₀	300	98%	47 100	39 000	1.92

^{a)} Calculated using Equation 2; ^{b)} Determined using DMF–SEC.

relative functionalization efficiency. We observed that grafts with DP100 *N*-acryloylmorpholine (NAM) from the BDD-3AP-mCCTA PBAE produced with 6 eq. NHS–PABTC and 3 eq. TEA yielded monomodal NAM₅₀–(BDD-3AP)–NAM₅₀ ABA ternary graft copolymers suggesting complete functionalization on both end groups. In contrast, graft copolymers prepared with <5 eq. NHS–PABTC and <3 eq. TEA yielded bimodal molar mass distributions suggesting incomplete RAFT agent functionalization (Figure 2b). PBAE functionalization was further verified by M_{n, SEC} with an increase from 9500 Da for BDD-3AP-mCCTA to masses of ≈20 000 for the partially functionalized polymers and an M_{n, SEC} of 30 200 for fully functionalized NAM₅₀–(BDD-3AP)–NAM₅₀. We therefore proceeded with 6 eq. of TEA and 3 eq. of NHS–RAFT as the selected method parameters. Kinetic analysis of the polymerization of BDD-3AP-mCCTA and HDD–PIP–mCCTA with the NAM monomer showed over 90% monomer conversion was achieved within 4 h with a gradual increase in molar mass observed (Figures S2 and S3, Supporting Information).

Following the optimization of the grafting-from methodology we sought to explore the synthetic versatility of the platform by expanding the monomer set for the RAFT polymerization step. Accordingly, we employed a range of five vinyl monomers, two neutral charge monomers (NAM and dimethylacrylamide (DMA)), two negatively charged monomers (2-acrylamidopropanesulfonate (AMPS) and acrylic acid (AA)), and a positively charged monomer (*N,N'*-dimethylaminoacrylate (DMAEA)), to extend both HDD–PIP and BDD-3AP PBAE-mCCTAs, targeting a DP of 100 at both ends of the PBAE–mCCTA in each case (Table 2). We found the RAFT polymerization only achieved high conversion rates (>90%) for neutral monomers, with the negative and positively charged monomers yielding low monomer conversion. We expect this may be due to poor solubility of the AMPS monomer in solvents appropriate for the PBAE–mCCTAs and acidic degradation of the PBAE–mCCTAs by the AA and AMPS monomers, verified by ¹H NMR spectroscopy showing the disappearance of the polyester signal present at around

4 ppm following HDD–PIP–mCCTA RAFT with AA and BDD-3AP-mCCTA RAFT with AMPS (Figures S4 and S6, Supporting Information).

Another key advantage of our grafting-from process is that the RAFT polymerization step enables the precise control of the graft lengths and therefore control over final copolymer molecular mass. To exemplify this, we performed graft-copolymerizations with both DMA and NAM monomers at DP100, 200, and 300 by varying the (vinyl monomer)/(PABTC–mCCTA) ratio (Table 2), (Figures 2a,b). All polymerizations achieved conversions above 90% with SEC chromatograms exhibiting higher molar mass polymers with increasing target chain length (Figure 3c; Figure S5, Supporting Information).

3.2. Assembly of Polymeric Nanoparticles

We have demonstrated the ability to produce a range of triblock graft copolymers utilizing the PBAE–mCCTA platform. Given the extensive use of PBAEs as biomaterials, we hypothesized that such block copolymers may have potential as a drug delivery platform. Given their hydrophobic PBAE central block and hydrophilic coronas, we initially tested the ability of NAM₅₀–(BDD-3AP)–NAM₅₀, DMA₅₀–(BDD-3AP)–DMA₅₀, NAM₅₀–(HDD-PIP)–NAM₅₀, and DMA₅₀–(HDD-PIP)–DMA₅₀ copolymers to form block copolymer micelle assemblies. Micelle formation was conducted through a solvent precipitation methodology, using tetrahydrofuran or acetone as the organic solvent applied to solubilize the polymer, followed by its dropwise addition to stirring water and subsequent removal of organic solvent by evaporation. It was determined that polymers based on a BDD-3AP core were not suitable for particle assembly, with the polymer either not forming particles (DMA copolymer) or forming unstable particles (NAM copolymer). Stability was assessed through particle addition to ionic media (phosphate buffer saline at pH 7.4), with a rapid aggregation of the NAM₅₀–(BDD-3AP)–

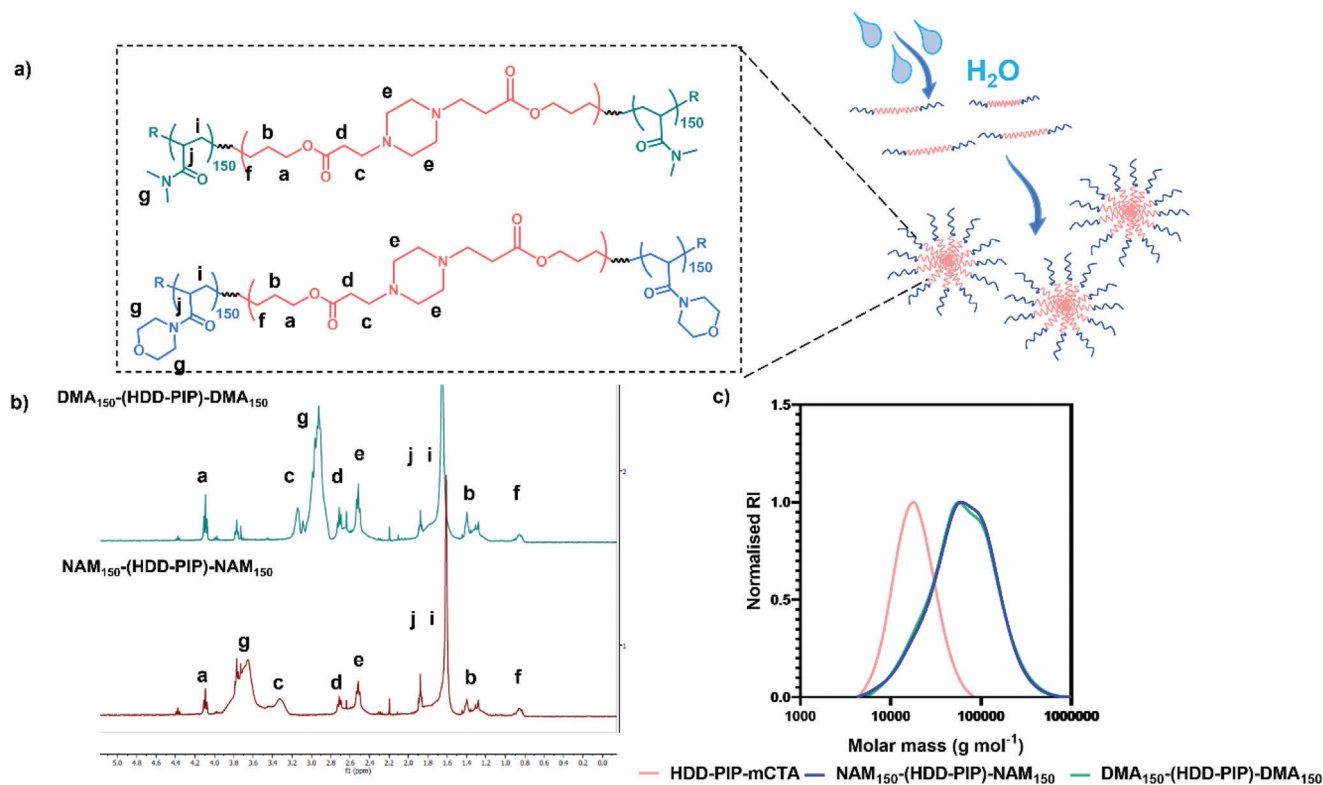


Figure 3. Polymer characterization of NAM_{150} -(HDD-PIP)- NAM_{150} and DMA_{150} -(HDD-PIP)- DMA_{150} : a) Structures of both polymers; b) ^1H NMR spectra in CDCl_3 ; c) Molar mass distribution (g mol^{-1}) of the obtained polymers and the starting PBAE-mCTA.

NAM_{50} particles observed, confirmed by an increase in particle diameter from below 200 nm to above 1000 nm.

Meanwhile block copolymers derived from the HDD-PIP PBAE-mCTA produced particles with mean diameters of 207 and 227 nm for NAM_{50} -(HDD-PIP)- NAM_{50} and DMA_{50} -(HDD-PIP)- DMA_{50} , respectively, which showed no observable aggregation when diluted in PBS (Figure S7, Supporting Information). For both particle types, the sample polydispersity (PDI) was below 0.3, with NAM_{50} -(HDD-PIP)- NAM_{50} showing a mean PDI of 0.19 and DMA_{50} -(HDD-PIP)- DMA_{50} NPs a mean PDI of 0.25. A monomodal particle size distribution by intensity was observed for each particle type. We hypothesized that this enhanced stability was due to the greater hydrophobicity of HDD-PIP, compared to BDD-3AP, enhancing the nonpolar interactions and thus stabilizing the resulting particles.

We sought to optimize this formulation process to produce smaller nanoparticles, ideally below 200 nm as these have been shown to have improved uptake to tumor cells and enhanced biofilm penetration, two potential applications for these materials.^[22–24] Furthermore, eliminating the use of organic solvents may also improve the translation of these materials.^[25] We therefore sought to solubilize directly the prepared HDD-PIP polymers in water without the use of organic solvent (Figure 3a). This was performed through direct water addition to dry polymer powder, followed by stirring for 1 h. We found that while for the NAM_{50} -(HDD-PIP)- NAM_{50} and DMA_{50} -(HDD-PIP)- DMA_{50} polymers direct assembly was not possible, for NAM_{100} -(HDD-PIP)- NAM_{100} , NAM_{150} -(HDD-PIP)- NAM_{150} , DMA_{100} -

(HDD-PIP)- DMA_{100} , and DMA_{150} -(HDD-PIP)- DMA_{150} polymers, we achieved spontaneous particle assembly following water addition. We hypothesized this result from the longer hydrophilic RAFT chains in the latter promoting polymer water solubility and particle assembly. The diameters of the particles obtained through direct polymer solubilization, were in each case below 200 nm, with a mean diameter of 127 nm reported for NAM_{150} -(HDD-PIP)- NAM_{150} and 120 nm for DMA_{150} -(HDD-PIP)- DMA_{150} (Figure 4b). Sample PDI were 0.26 and 0.24 for NAM_{150} -(HDD-PIP)- NAM_{150} and DMA_{150} -(HDD-PIP)- DMA_{150} , respectively. DMA_{150} -(HDD-PIP)- DMA_{150} particles gave a monomodal size distribution by intensity, ranging from 40 to 460 nm, while for NAM_{150} -(HDD-PIP)- NAM_{150} NPs two particle populations were observed, one ranging from 10 to 40 nm and the other from 40 to 500 nm (Figure 4c). TEM images provided further evidence the diameters for both the polymer variants were below 200 nm (Figure 4a).

Given the potential application of these materials in a biomedical context we assessed particle stability in water, at room temperature across 48 h, to evaluate whether particle aggregation occurs. DMA_{150} -(HDD-PIP)- DMA_{150} showed a decrease of mean diameter from 120 to 56 nm, while NAM_{150} -(HDD-PIP)- NAM_{150} particles retained a mean diameter of 128 nm throughout the stability study (Figure 4b). For each NP type, a decrease in particle PDI was observed (from 0.26 to 0.13 and from 0.24 to 0.17 for NAM_{150} -(HDD-PIP)- NAM_{150} and DMA_{150} -(HDD-PIP)- DMA_{150} , respectively). For both types of polymer particles, aggregation was not observed. The reduction in particle size for

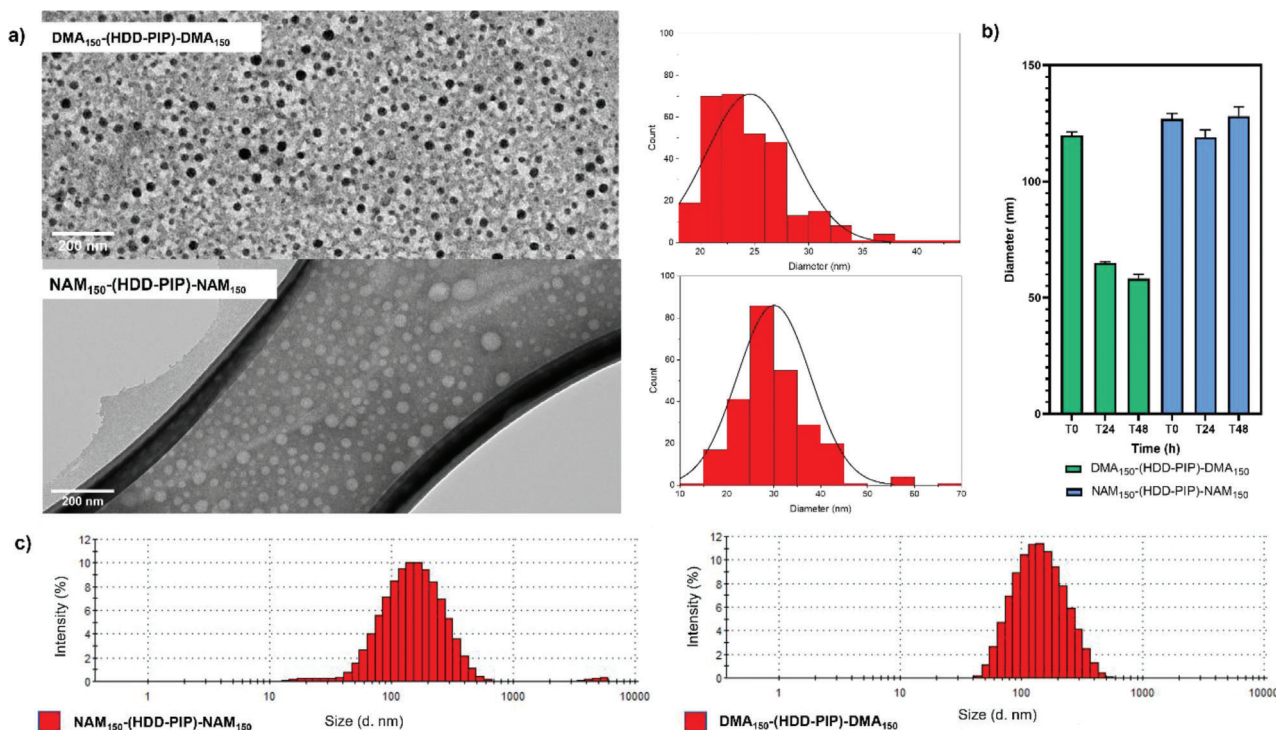


Figure 4. Particle characterization of NAM₁₅₀-(HDD-PIP)-NAM₁₅₀ and DMA₁₅₀-(HDD-PIP)-DMA₁₅₀: a) TEM particle size distribution (nm) and TEM images of uranyl acetate-stained NPs on Formvar carbon 200 mesh grid for DMA₁₅₀-(HDD-PIP)-DMA₁₅₀ particles or a graphene oxide grid for NAM₁₅₀-(HDD-PIP)-NAM₁₅₀ particles, scale bar at 200 nm; b) Particle diameter (nm) across 48 h, at room temperature, in water at 1 mg mL⁻¹; c) Particle size (nm) distribution by intensity (%) in water, at room temperature, at 1 mg mL⁻¹.

the DMA₁₅₀-(HDD-PIP)-DMA₁₅₀ triblock copolymer may be due to the particles initially resolving in a kinetically trapped state and slowly reconfiguring into smaller nanoparticles during the course of the stability study.^[26]

3.3. Drug Encapsulation and In Vitro Release

We next evaluated the potential of NAM₁₅₀-(HDD-PIP)-NAM₁₅₀ and DMA₁₅₀-(HDD-PIP)-DMA₁₅₀ micelles as delivery vehicles for hydrophobic drug molecules. Docetaxel (DTX) was selected as the hydrophobic drug of choice due to its low solubility in water and bulky polycyclic structure, combined with high activity in most cancer cell lines.^[27]

DTX encapsulation was achieved through simultaneous addition of water and a drug solution in DMSO (Figure 5a), to weighed out dry polymer, followed by stirring for 2 h and subsequent removal of unencapsulated DTX by centrifugal filtration. This yielded a mean drug load of 10% ± 2.6% and 11% ± 2.8% for DMA₁₅₀-(HDD-PIP)-DMA₁₅₀ and NAM₁₅₀-(HDD-PIP)-NAM₁₅₀, respectively, across three experimental replicates, demonstrating polymer suitability for hydrophobic drug encapsulation (Figure 5b). A negligible change in mean particle diameter and polydispersity following DTX encapsulation was observed for both particle variants tested (Figure 5c,d). The findings suggest our block copolymer micelle assemblies are suitable for the delivery of hydrophobic drug molecules.

In vitro release of DTX from NAM₁₅₀-(HDD-PIP)-NAM₁₅₀ and DMA₁₅₀-(HDD-PIP)-DMA₁₅₀ micelles was evaluated in

phosphate buffer at pH 7.4 (blood pH) simulating body temperature (37 °C; Figure 5e). NAM₁₅₀-(HDD-PIP)-NAM₁₅₀ particles achieved 32% drug release within the first 5 h, reaching 52% following 24 h. DTX release from DMA₁₅₀-(HDD-PIP)-DMA₁₅₀ micelles was initially slower, reaching 20% after 5 h followed by an increase to 69% after 24 h. Following 48 h DTX release from DMA₁₅₀-(HDD-PIP)-DMA₁₅₀ increased to 76%, followed by a reduction in the percentage of cumulative release to 68% following 72 h, hypothesized to originate from the hydrolysis of DTX ester bonds. A drop in DTX cumulative release from the NAM₁₅₀-(HDD-PIP)-NAM₁₅₀ polymer was also observed with a reduction from 52% observed after 24 h to 47% at 72 h. Comparatively, the free drug control achieved only 44% cumulative drug release following 24 and 72 h due to the limited solubility of DTX. Following DTX encapsulation in both NAM₁₅₀-(HDD-PIP)-NAM₁₅₀ and DMA₁₅₀-(HDD-PIP)-DMA₁₅₀ NPs an improvement in drug solubility was observed, stipulated to originate from the nano size of the particles influencing the solubility and dissolution rate of DTX through decreased particle size and increased surface area, as described by the Kevin and Noyes-Whitney equations.^[28,29]

3.4. Uptake in 2D Monolayers of MDA-MB-231 Breast Cancer Cells

Effective drug delivery systems are pivotal in enhancing therapeutic outcomes in cancer treatment,^[30] with nanomaterials emerging as promising candidates for targeted drug delivery in

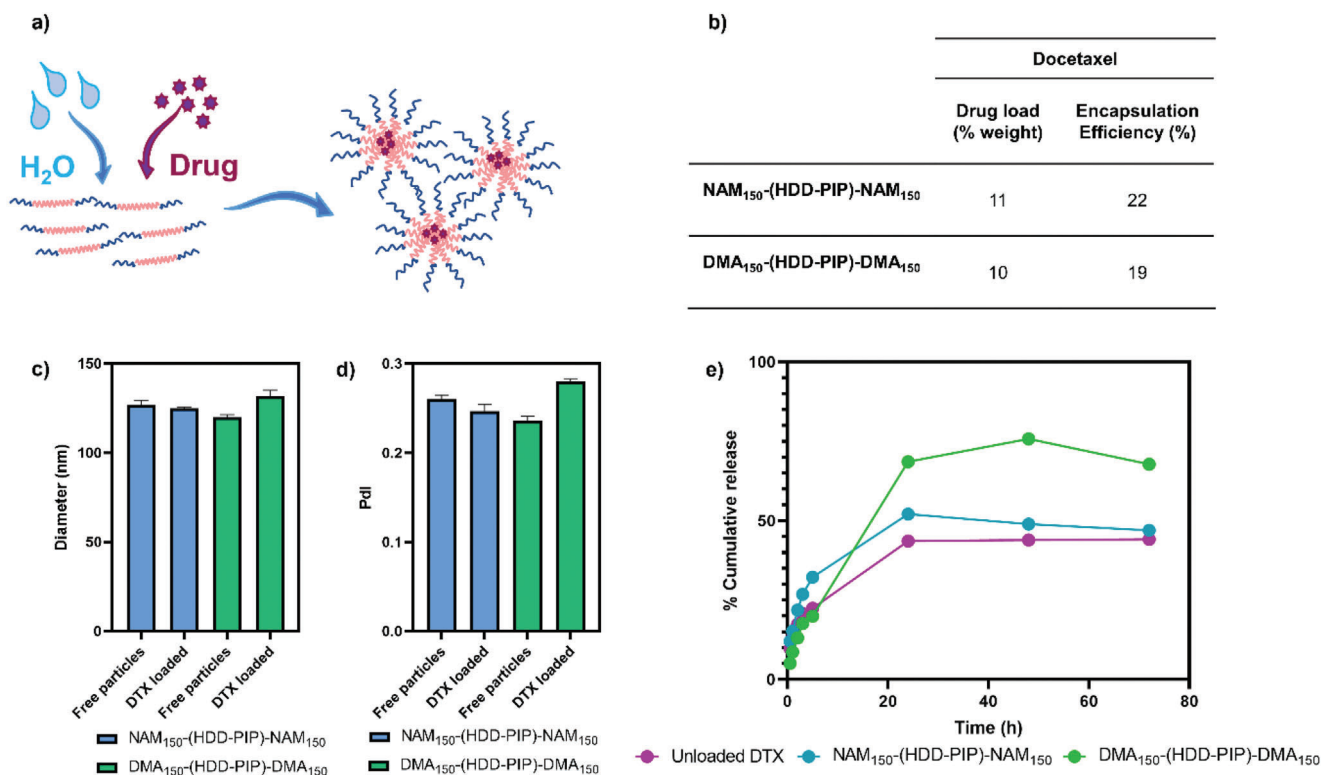


Figure 5. Drug encapsulation in NAM₁₅₀-(HDD-PIP)-NAM₁₅₀ and DMA₁₅₀-(HDD-PIP)-DMA₁₅₀ particles, where: a) Scheme of DTX loading in PBAE-RAFT particles b) Inset table that describes cumulative drug load (%) and encapsulation efficiency of DTX, defined by HPLC; c) Change in mean particle diameter (nm) following DTX encapsulation, in water at 1 mg mL⁻¹ where average diameter for DTX loaded particles is 125 nm for NAM₁₅₀-(HDD-PIP)-NAM₁₅₀ and 132 nm DMA₁₅₀-(HDD-PIP)-DMA₁₅₀; d) Change in particle PDI following DTX encapsulation, in water at 1 mg mL⁻¹ where average PDI for NAM₁₅₀-(HDD-PIP)-NAM₁₅₀ is 0.26 and 0.24 for DMA₁₅₀-(HDD-PIP)-DMA₁₅₀ for DTX loaded particles is 0.25 for NAM₁₅₀-(HDD-PIP)-NAM₁₅₀ and 0.28 DMA₁₅₀-(HDD-PIP)-DMA₁₅₀; e) DTX release from NAM₁₅₀-(HDD-PIP)-NAM₁₅₀ (blue) and DMA₁₅₀-(HDD-PIP)-DMA₁₅₀ (green) particles and unloaded DTX (purple) in phosphate buffer pH 7.4, containing 0.25% Tween 20, at 37 °C, across 72 h, samples analyzed by HPLC.

cancer therapy.^[31] Hence, we investigated the cellular uptake and lysosomal co-localization of rhodamine functionalized NAM₁₅₀-(HDD-PIP)-NAM₁₅₀ and DMA₁₅₀-(HDD-PIP)-DMA₁₅₀ NPs in MDA-MB-231 breast cancer cells. Successful cellular uptake and preferential localization in lysosomes are crucial factors for ensuring efficient drug delivery and effective treatment outcomes.^[31,32] Our results demonstrated a robust cellular uptake of the nanoparticles within breast cancer cells. Confocal microscopy revealed a clear distribution of nanoparticles throughout the cytoplasm, confirming their successful internalization as illustrated in **Figure 6**. Furthermore, the assessment of co-localization demonstrated a significant degree of overlap between the nanoparticles and lysosomes, with a Pearson correlation coefficient of 0.5 for each nanoparticle system. This finding indicates that a substantial proportion of the NPs are trafficked to the lysosomes, suggesting their potential utilization as templates for drug delivery, considering lysosomes are key organelles involved in nanoparticle degradation and effective release of the payload.^[33] This promising result opens avenues for future studies to explore the use of these copolymers for the delivery of a range of chemotherapeutic agents and further elaborate on the precise mechanisms underlying the lysosomal accumulation and subsequent release of drugs from these NPs.

3.5. Cytotoxicity Assessment of Nanoparticles in 2D Monolayers of MDA-MB-231 Breast Cancer Cells

The cytotoxic activity of NAM₁₅₀-(HDD-PIP)-NAM₁₅₀ and DMA₁₅₀-(HDD-PIP)-DMA₁₅₀ were assessed in vitro on MDA-MB-231 breast cancer cells using the PrestoBlue Cell Viability Reagent. Both particles demonstrated cellular viability above 80% across all concentrations, indicating the biocompatibility of these polymers when used with cells at the tested concentrations (Figure S9, Supporting Information). Our findings suggest that these NPs could serve as potential platforms for loading chemotherapeutic agents, allowing for the management of various cancer types.

4. Conclusion

We report a new grafting-from methodology to functionalize PBAEs with neutrally charged RAFT monomers, to obtain ABA tri-block copolymers at a range of DPs and with monomodal molar mass distributions. We demonstrate successful NP assembly of selected materials, NAM₁₅₀-(HDD-PIP)-NAM₁₅₀ and DMA₁₅₀-(HDD-PIP)-DMA₁₅₀, obtaining particle sizes below 200 nm and achieving over 10% drug loading of the model hydrophobic drug, DTX. Rhodamine tagged NAM₁₅₀-(HDD-PIP)-

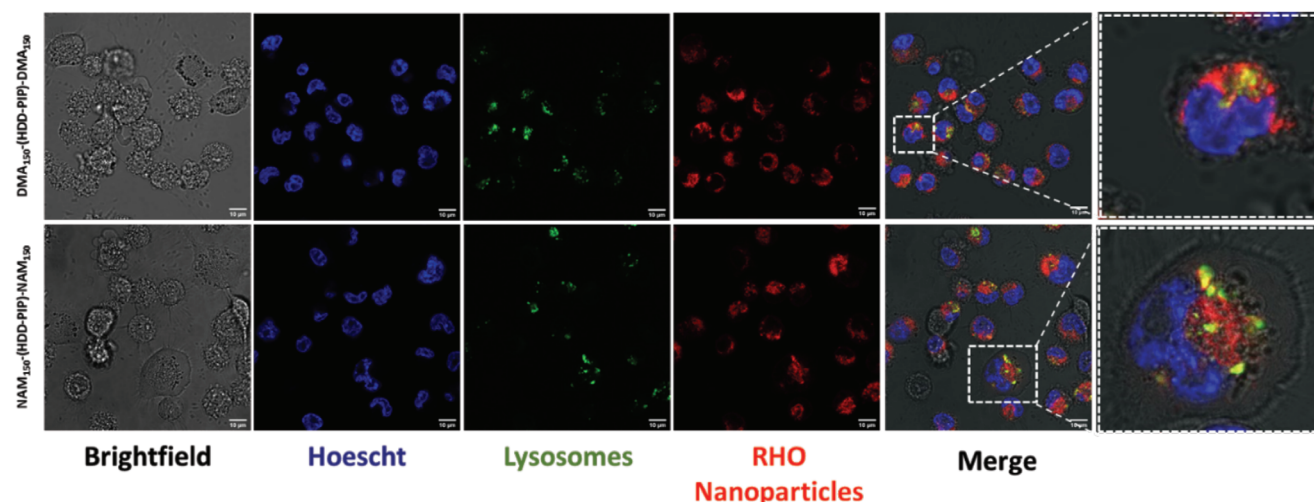


Figure 6. Nanoparticle uptake studies: a) Confocal microscopy imaging at 63× illustrating the cellular uptake of rhodamine labelled NAM₁₅₀–(HDD-PIP)–NAM₁₅₀ and DMA₁₅₀–(HDD-PIP)–DMA₁₅₀ nanoparticles in MDA-MB-31 breast cancer cell lines and their co-localization within lysosomes (Lumi-Tracker Lyso Green). Scale bar = 10 μm. The image contrast was enhanced through saturating the pixels by 0.1% using the “enhance contrast” feature in ImageJ across all channels and the original images attached in Figure S8 (Supporting Information).

NAM₁₅₀ and DMA₁₅₀–(HDD-PIP)–DMA₁₅₀ particles were shown to be successfully internalized in MDA-MB-231 breast cancer cells, particularly in lysosomes, demonstrating a potential application as vehicles for therapeutic drug delivery.

Our findings facilitate the preparation of structurally diverse ABA tri-block PBAE–RAFT copolymers, therefore expanding the scope of PBAEs and introducing a new class of biomaterial. Considering the plethora of neutral acrylate and acrylamide monomers that can be attached through the RAFT process, copolymer properties can now be finely tuned to tailor them for selected applications. Moreover, precise control over the final RAFT polymer DPs may offer bespoke ways of controlling end polymer properties, facilitating NP design to tailor drug release profiles, enhance stability in physiological fluids, and target specific cell types and environments. Furthermore, considering the successful encapsulation of DTX, the developed polymeric micelles can be applied for the oral delivery of a range of hydrophobic drugs, by enhancing their bioavailability, through improvement of solubility, permeability, and dissolution rate. This can be particularly expanded to deliver drug combination therapies by achieving enhanced therapeutic efficacy.

Supporting Information

Supporting Information is available from the Wiley Online Library or from the author.

Acknowledgements

M.C. and K.H. are funded by the National Biofilms Innovation Centre (NBIC) that is an innovation and knowledge center funded by the Biotechnology and Biological Sciences Research Council, Innovate UK and Hartree Centre [Awards Numbers BB/R012415/1 and BB/X002950/1]. The authors thank the Royal Society (Wolfson Research Merit Award WM150086 to C.A.). The authors also thank Tom Hyde, Esme Ireson, and Paul Cooling for expert technical support. The Nanoscale & Macroscale

Research Centre (NMRC) is acknowledged for providing the facilities for TEM and related analysis. The authors thank the School of Life Sciences Imaging facility (SLIM) and their staff for the use of their facilities. K.K. was funded by Wellcome Trust AAMR DTP program (grant 108876/Z/15/Z).

Conflict of Interest

The authors declare no conflict of interest.

Data Availability Statement

The data that support the findings of this study are available from the corresponding author upon reasonable request.

Keywords

biomaterials, grafting-from, hydrophobic drug delivery, poly(β -amino esters), RAFT, Triblock copolymer

Received: July 21, 2023

Revised: August 25, 2023

Published online:

- [1] D. M. Lynn, R. Langer, *J. Am. Chem. Soc.* **2000**, *122*, 10761.
- [2] Y. Liu, Y. Li, D. Keskin, L. Shi, *Adv. Healthcare Mater.* **2019**, *8*, e1801359.
- [3] Y. Liu, H. J. Busscher, B. Zhao, Y. Li, Z. Zhang, H. C. Van Der Mei, Y. Ren, L. Shi, *ACS Nano* **2016**, *10*, 4779.
- [4] J. J. Green, R. Langer, D. G. Anderson, *Acc. Chem. Res.* **2008**, *41*, 749.
- [5] X. Su, J. Fricke, D. G. Kavanagh, D. J. Irvine, *Mol. Pharm.* **2011**, *8*, 774.
- [6] J. Wei, L. Zhu, Q. Lu, G. Li, Y. Zhou, Y. Yang, L. Zhang, *J. Control. Release* **2023**, *354*, 337.
- [7] Y. Zhang, R. Wang, Y. Hua, R. Baumgartner, J. Cheng, *ACS Macro Lett.* **2014**, *3*, 693.

- [8] J. Karlsson, K. R. Rhodes, J. J. Green, S. Y. Tzeng, *Expert Opin. Drug Deliv.* **2020**, *17*, 1395.
- [9] C. Zhang, T. An, D. Wang, G. Wan, M. Zhang, H. Wang, S. Zhang, R. Li, X. Yang, Y. Wang, *J. Control. Release* **2016**, *226*, 193.
- [10] J. Kim, S. K. Mondal, S. Y. Tzeng, Y. Rui, R. Al-Kharboosh, K. K. Kozielski, A. G. Bhargav, C. A. Garcia, A. Quiñones-Hinojosa, J. J. Green, *ACS Biomater. Sci. Eng.* **2020**, *6*, 2943.
- [11] J. Kim, Y. Kang, S. Y. Tzeng, J. J. Green, *Acta Biomater.* **2016**, *41*, 293.
- [12] T. Thambi, V. H. Giang Phan, S. H. Kim, T. M. Duy Le, H. T. T. Duong, D. S. Lee, *Biomater. Sci.* **2019**, *7*, 5424.
- [13] R. A. Cordeiro, D. Farinha, N. Rocha, A. C. Serra, H. Faneca, J. F. J. Coelho, *Macromol. Biosci.* **2015**, *15*, 215.
- [14] S. C. Larnaudie, J. C. Brendel, K. A. Jolliffe, S. Perrier, *J. Polym. Sci. A Polym. Chem.* **2016**, *54*, 1003.
- [15] D. Roy, J. T. Guthrie, S. Perrier, *Macromolecules* **2005**, *38*, 10363.
- [16] P. De, M. Li, S. R. Gondi, B. S. Sumerlin, *J. Am. Chem. Soc.* **2008**, *130*, 11288.
- [17] G. Moad, Y. K. Chong, A. Postma, E. Rizzardo, S. H. Thang, *Polymer* **2005**, *46*, 8458.
- [18] C. J. Ferguson, R. J. Hughes, B. T. T. Pham, B. S. Hawkett, R. G. Gilbert, A. K. Serelis, C. H. Such, *Macromolecules* **2002**, *35*, 9243.
- [19] N. S. Bhise, R. S. Gray, J. C. Sunshine, S. Htet, A. J. Ewald, J. J. Green, *Biomaterials* **2010**, *31*, 8088.
- [20] P. S. Kumbhar, S. K. Diwate, U. G. Mali, T. U. Shinde, J. I. Disouza, A. S. Manjappa, *Ann. Pharm. Fr.* **2020**, *78*, 398.
- [21] S. Bolte, F. P. Cordelières, *J. Microsc.* **2006**, *224*, 213.
- [22] Y. H. Bae, K. Park, *J. Control. Release* **2011**, *153*, 198.
- [23] S. A. Kulkarni, S.-S. Feng, *Pharm. Res.* **2013**, *30*, 2512.
- [24] K. Forier, A.-S. Messiaen, K. Raemdonck, H. Nelis, S. De Smedt, J. Demeester, T. Coenye, K. Braeckmans, *J. Control. Release* **2014**, *195*, 21.
- [25] M. R. Mozafari, *Cell Mol. Biol. Lett.* **2005**, *10*, 711.
- [26] Y. Wang, J. He, C. Liu, W. H. Chong, H. Chen, *Angew. Chem., Int. Ed.* **2015**, *54*, 2022.
- [27] Y. Mi, Y. Liu, S.-S. Feng, *Biomaterials* **2011**, *32*, 4058.
- [28] A. A. Noyes, W. R. Whitney, *J. Am. Chem. Soc.* **1897**, *19*, 930.
- [29] K. G. Nelson, *J. Pharm. Sci.* **1972**, *61*, 479.
- [30] R. S. Riley, C. H. June, R. Langer, M. J. Mitchell, *Nat. Rev. Drug Discovery* **2019**, *18*, 175.
- [31] X. Kong, Y. Qi, X. Wang, R. Jiang, J. Wang, Y. Fang, J. Gao, K. Chu Hwang, *Prog. Mater. Sci.* **2023**, *134*, 101070.
- [32] M. A. Raheem, M. A. Rahim, I. Gul, X. Zhong, C. Xiao, H. Zhang, J. Wei, Q. He, M. Hassan, C. Y. Zhang, D. Yu, V. Pandey, K. Du, R. Wang, S. Han, Y. Han, P. Qin, *OpenNano* **2023**, *12*, 100152.
- [33] M. Chountoules, D. R. Perinelli, A. Forys, V. Chrysostomou, A. Kaminari, G. Bonacucina, B. Trzebicka, S. Pispas, C. Demetzos, *Int. J. Pharm.* **2023**, *630*, 122440.